Available online at www.sciencedirect.com

ScienceDirect

Advances in Space Research 72 (2023) 47–64

ADVANCES IN SPACE RESEARCH (a COSPAR publication)

www.elsevier.com/locate/asr

On precise orbit determination based on DORIS, GPS and SLR using Sentinel-3A/B and -6A and subsequent reference frame determination based on DORIS-only

Patrick Schreiner *, Rolf König, Karl Hans Neumayer, Anton Reinhold

Helmholtz Centre Potsdam GFZ German Research Centre for Geosciences, Claude-Dornier-Straße 1, D-82234 Weßling, Germany

Received 30 April 2022; received in revised form 29 March 2023; accepted 2 April 2023
Available online 13 April 2023

Abstract

The Helmholtz-Zentrum Potsdam GFZ German Research Centre for Geosciences is one of the Associate Analysis Centers of the International Doppler Orbitography and Radiopositioning Integrated by Satellite (DORIS) Service (IDS). In the framework of a recent reprocessing campaign for the International Terrestrial Reference Frame (ITRF) the suite of DORIS-derived satellite products was extended and improved with respect to reference frame determination. Among others the Copernicus Sentinel-3A/3B and 6A Michael Freilich (MF) satellites were used for this purpose. The orbits were generated based on DORIS-only and on the combination of DORIS and Satellite Laser Ranging (SLR) observations, and attempts were made to optimize their accuracy. Also for these satellites, GFZ generates Global Positioning System (GPS) based orbits within the Copernicus Precise Orbit Determination (CPOD) quality working group (CPOD-QWG). The GPS orbits contribute to a combined CPOD orbit solution, which is assumed to have superior absolute accuracy and minimal residual systematic errors. The DORIS-only, the combined DORIS and SLR, and the GPS-only orbits are compared to the CPOD combined solution serving as reference solution. The accuracy of the orbits shows up in radial direction for all techniques and combinations with values of 0.60 to 0.82 cm. In transverse and normal direction the RMS values achieved with GPS are up to around 50% lower as with DORIS, which sizes at around 1.5–2 cm. Subsequently the reference points of the observation techniques were estimated. With a multi-technique approach, a center-of-mass deviation according to Montenbruck et al. (2017) could be reproduced for Sentinel-3A. In addition, for both Sentinel-3 satellites the DORIS reference point values show a deviation in normal direction of 8–9 mm and a drift in radial direction of about 3 mm/year with respect to manufacturer's data, reference point values for Sentinel-6A (MF) show a good agreement. With the confidence gained on the DORIS-only orbit solutions, weekly local reference frames are computed for each of the three satellites as well as a combined solution and evaluated in terms of the reference frame defining parameters, i.e. origin, scale, and orientation. The accuracy achieved here is in the range of a few mm to cm region. The scale remains stable, except for Sentinel-3A, which shows a scale drift of about −1.5 mm/year, whose cause is not clear yet. Standard deviations of station coordinate residuals (North, East, Up) are in the range of 2–4 mm, 5–9 mm and 5–7 mm respectively.

Keywords: DORIS; GPS; SLR; Precise orbit determination; Sentinel; Reference frame; Time bias

1. Introduction

The Sentinel satellites Copernicus Sentinel-3A (S3A), Sentinel-3B (S3B) and Sentinel-6A Michael Freilich (S6A) (ESA, 2021; Donlon et al., 2021) are three altimetry mission satellites operated by the European Space Agency

* Corresponding author.
E-mail addresses: patrick.schreiner@gfz-potsdam.de (P. Schreiner), rolf.koenig@gfz-potsdam.de (R. König), neumayer@gfz-potsdam.de (K. H. Neumayer), reinh_a@gfz-potsdam.de (A. Reinhold).

https://doi.org/10.1016/j.asr.2023.04.002
0273-1177/

(ESA) and the European Organization for the Exploration of Meteorological Satellites (EUMETSAT), and respectively for S6A also by the National Aeronautics and Space Administration (NASA) and the National Oceanic and Atmospheric Administration (NOAA), in the framework of the Copernicus Earth observation program of the European Commission and ESA for Earth and climate observation. These three satellites are all equipped with three of the main space geodetic techniques, i.e. Doppler Orbitography and Radiopositioning Integrated by Satellite (DORIS), Global Navigation Satellite Systems (GNSS) and Satellite Laser Ranging (SLR). S3A and S3B are both structurally identical, the later on launched S6A satellite has a different satellite body geometry, and it orbits at a higher altitude and a lower inclination (see Table 1). GFZ as a member of the CPOD-QWG operationally contributes GPS based orbits for these satellites which are used for a most precise combination of all the solutions (GMV, 2022a).

The software continuously developed and extended at GFZ for Precise Orbit Determination (POD) is the software EPOS-OC (Zhu et al., 2004). Besides GNSS-derived orbital products, this software was also previously used for DORIS-related studies using observations in the DORIS Doppler V2 format (CNES, 2008) in f.i. (Rudenko et al., 2017) and also using observations given in the Receiver INdependent EXchange (RINEX) format (CNES, 2022b) in (König et al., 2021). Its features are continuously extended and augmented and can fully follow the IERS 2010 conventions (Luzum and Petit, 2012 and Petit and Luzum, 2010). Being quite an universal tool, it is used for POD, among other applications. It is capable of handling the four main space geodetic techniques: the three already mentioned ones and additionally Very Long Baseline Interferometry (VLBI).

In the framework of ITRF determination GFZ contributes with EPOS-OC derived products as an International Laser Ranging Service (ILRS) (Pearlman et al., 2019) Analysis Center contributing to the SLR part. As an International DORIS Service (IDS) (Willis et al., 2015) Associate Analysis Center GFZ is currently on a non regular basis contributing development solutions for evaluation with the objective to prospectively contribute to the DORIS part to the ITRF (Moreaux et al., 2016). For the purpose of the ITRF2020 development, GFZ extended and reprocessed the suite of DORIS based products, motivated by permanent quality control with external solutions or in–house multi technique comparisons. With that in mind, EPOS-OC is maintained to meet the latest state-of-the art scientific achievements and requirements.

Table 1
Orbital characteristics of the Sentinel satellites.

	Height of the perigee	Inclination	Numerical eccentricity	Launch
Sentinel-3A	794 km	98.7°	0.0014	16-Feb-2016
Sentinel-3B	794 km	98.7°	0.0014	25-Apr-2018
Sentinel-6A	1336 km	65.9°	0.0006	21-Nov-2020

In this study we analyze the latest orbit products generated with EPOS-OC using the techniques DORIS in combination with SLR, DORIS-only and GPS-only. We compare the obtained orbits with the combined orbits (GMV, 2022a) and also independently via SLR. Therefore we assess statistical key figures as well as the two-dimensional distribution of orbital differences on the sphere. Based on these orbits, the reference points of the DORIS antennas are estimated and compared with post-launch estimated values provided by the IDS to see if same adjustments can be verified. Subsequently we use the DORIS-only solutions and solve on a weekly basis for DORIS station coordinates and daily pole coordinates and length-of-day (LOD). The quantities thus obtained are evaluated compared to a priori based on the reference frame defining parameters, i.e. origin, scale, and orientation.

2. Orbit determination procedure

2.1. Software and model definition

The software used for POD is GFZ's Earth Parameter and Orbit System (EPOS) in the core module for Orbit Computation called EPOS-OC (Zhu et al., 2004). This software is capable of processing and simulating the four main space geodetic observation techniques. In this study, we use SLR, DORIS, and GNSS observations. We use DORIS, SLR and GNSS ground observations as obtainable from the Crustal Dynamics Data Information System (CDDIS) (Noll (2010), Noll et al. (2018)) and from the EUROLAS Data Center (EDC) (Schwatke, 2012). DORIS observations, starting with Jason-2, are given in the RINEX format. To handle RINEX observations with EPOS-OC a preprocessing procedure was implemented, which is in the first step based on the procedure developed by (Lemoine, 2014) for the GINS (Geodesie par Integrations Numeriques Simultanees) software (Further information can be found in Lemoine et al. (2016)). In this step, first Doppler count measurements are obtained. For this purpose, the ionosphere-free linear combinations of the phase signals are generated and the difference of two consecutive 10-s measurements is formed. 3-s measurements are not used here. In order to use the same input channel for observation data with EPOS-OC as with conventional DORIS observations in the standard Exchange Format, these Doppler count measurements must be converted to DORIS Range-Rate measurements. For this purpose, the observation equation corresponding to the DORIS Exchange Format description (CNES (2008)) is used (see also f.i. Zelensky et al. (2006)):

$$DRR = c * (1 + \Delta f_{beac}) * \frac{1}{f_{beac}} * (-1)\frac{N_c}{\Delta t} \quad (1)$$

with:

DRR - DORIS range-rate measurement

c - speed of light
Δf_{beac} - Ground beacon frequency bias
f_{beac} - Nominal ground beacon frequency (for frequency shift faktor k = 0, f_{beac} corresponds to 2.03625 GHz)
N_c - Number of cycles
Δt - Doppler count interval duration

It should be noted that, unlike range-rate observations in the standard exchange format, these measurements refer to the ionosphere-free reference points.

EPOS-OC uses cycle measurements as a computed observable. Therefore it is given as the distance differences at the start and end point of the Doppler integration time interval as multiples of the underlying wavelength of the beacon frequency:

$$zmes = \frac{(Dist_{t_1} - Dist_{t_2})}{\lambda} - \Delta t * \Delta_{f_{beac}} + \Delta_{Tropo} + \Delta_{Rela} - \Delta_{Phase} \quad (2)$$

with:

$Dist_{t_1}$ - Distance station to satellite at Doppler count start interval t_1
$Dist_{t_2}$ - Distance station to satellite at Doppler count end interval t_2
λ - Carrier wavelength of f_{beac}
$\Delta t * \Delta_{f_{beac}}$ - Beacon frequency correction
Δ_{Tropo} - Tropospheric correction
Δ_{Rela} - Relativistic correction
Δ_{Phase} - Phase correction

On the other hand the observed measurement, based on the range-rate measurement:

$$zmes = \Delta t * (f_{beac} * (1 - \frac{DRR}{c}) - f_{sat}) \quad (3)$$

with:

f_{sat_t} - Satellite frequency at epoch t (for t_0 the nominal f_{sat} corresponds to 2.036125 GHz)

In the case of GPS processing we use L1 and L2 code and phase observations of ground stations and LEO satellites. For Galileo+GPS processing we use E1 and E5 observations for Galileo. From code and phase observations we form the ionosphere-free linear combination (zero differenced). For GPS-derived orbits we use a two-step approach, whereby in the first step, the GPS constellation is solved for in a comprehensive network adjustment. In the second step, the GPS orbits and clock parameters are introduced into the LEO POD as fixed quantities. The constellation used for this is an especially generated solution, which for highest integrity follows the exact same models as for LEO POD. To that end, we use a ground station network of about 120 IGS14 stations that are globally distributed as evenly as possible. The constellation is solved over intervals of 30 h length, starting at 21:00 h UT the day before and ending at 03:00 h UT the day after. The reference time is slaved to a maser station whose clock is closest to IGS time. The GPS-based LEO POD is an ambiguity float solution with an arc length of 28 h starting at 22:00 h UT the day before and ending at 02:00 h UT the day after and cut to 24 h daily arcs (00:00 h UT to 00:00 h UT). LEO antenna phase center variation (PCV) maps are calibrated in-flight using the residual stacking approach (Jäggi et al., 2009) and applied afterwards. In the case of DORIS processing we estimate a frequency bias and drift per station per pass, as well as one troposphere refraction bias per station per pass. The onboard frequency drift is corrected using the estimated frequency offsets of the master beacons. For SLR we use optical phase maps, see e.g. Arnold et al. (2018), and solve for one range bias per station per arc, following e.g. Appleby et al. (2016). That allows us to handle possible remaining inconsistencies in measurement device reference points. Table 2 shows the measurement device eccentricities used. The coordinate directions refer to the frame of the satellite body. In order to be more illustrative, we have nevertheless used, in the header line of the table, the designations 'radial', 'transversal' and 'normal', for thus is the satellite approximatively oriented when in nominal attitude. As S6A performs yaw flip maneuvers, note that depending on the direction of flight, the RTN axes will flip (180 degree yaw-flip) and the translation depends on the initial adopted orientation for the implemented attitude control. The indications in the satellite fixed reference system are unambiguous. The three satellites are equipped with an GNSS antenna of the same type. According to the manufacturer the L_1, L_2, E_1 and E_5 Phase Center Offset (PCO) values for this antenna are 97 mm in zenith direction, and zero in the plane. As the values for the L_1 and the L_2 PCO coincide, the ionosphere-free PCO value that is thus derived is 97 mm, following the equation:

Table 2
Used technique wise reference points. +10 mm correction in normal direction according to Montenbruck et al. (2017) mentioned in brackets where applied. (GPS/GNSS values without PCO of 68 mm in zenith direction for S3A and S3B, for S6A 75 mm for GPS and 93 mm for Galileo).

	Radial [cm]	Transversal [cm]	Normal [cm]
Sentinel-3A	-Z (S/C)	-X (S/C)	-Y (S/C)
DORIS	−107.3	−156.9	7.3
GPS-1	79.4	−288.1	−19.0 (+10 mm appl.)
GPS-2	79.4	−288.1	21.0 (+10 mm appl.)
SLR	−80.1	−113.4	64.8 (+10 mm appl.)
Sentinel-3B	-Z (S/C)	-X (S/C)	-Y (S/C)
DORIS	−107.3	−156.9	7.3
GPS-1	79.4	−288.1	−20.0
GPS-2	79.4	−288.1	20.0
SLR	−80.1	−113.4	63.8
Sentinel-6A	-Z (S/C)	-X (S/C)	Y (S/C)
DORIS	−100.4	−162.5	40.0
GNSS-1	108.0	−247.5	0.0
GNSS-2	108.0	−287.5	0.0
SLR	−66.5	−162.5	−40.1

$$L_{iono.free}PCO = \frac{f_1^2}{(f_1^2 - f_2^2)} * L_1PCO - \frac{f_2^2}{(f_1^2 - f_2^2)} * L_2PCO \quad (4)$$

with:

f_1 - 1.57542 GHz
f_2 - 1.22760 GHz

These PCO values were post-launch estimated by the CPOD-QWG to be 68 mm for the Sentinel-3 satellites and for Sentinel-6A 75 mm for GPS and 93 mm for Galileo. Since the antennas of the three satellites are mounted on a plane on top of the satellite body, their zenith direction in the satellite fixed coordinate system (-Z for all three satellites) can be translated to the radial direction. Accordingly, the PCO value for all three satellites in the satellite fixed reference frame is only a PCO-Z value. Even though Sentinel-3A and 3B are structurally identical satellites, the A-unit was post launch found to have a center-of-mass deviation of 10 mm contradicting the manufacturer's information in normal direction (compare f.i. Montenbruck et al. (2017)). For GPS and SLR this correction is mentioned for the reference points of the techniques (see Table 2). For the two Sentinel-3 satellites we use the antenna "GPS-1" alone. The values used for the DORIS antenna are in each case the manufacturer values with no further correction applied for S3A. Sentinel-6A has three GNSS on-board antennas: two provided by RUAG (now Beyond Gravity), and the third for the TRIG receiver, provided by NASA/JPL (Montenbruck et al., 2021). The latter is used in the context of radio occultation measurements. In this study, we only used the RUAG antenna "GNSS-1".

The models and parameterizations for the dynamic orbit determination are listed in Table 3. Concerning the dynamic modelling, we use for GPS a more reduced-dynamic approach with more dense empirical parameters. In contrast, for the SLR and DORIS stand-alone adjustement, the modelling follows a dynamic approach. The orientation of the satellites was not done with models, but with appropriate quaternion data sets obtained from star tracker cameras. The orientation of the rotatable solar panels of the Sentinel-3 satellites, however, which was defined by a model that, given the satellite body orientation, always turns the solar panel normal towards the Sun. We use macromodels for the calculation of disturbance forces. The macromodel of the Sentinel-3 satellites is identical for the A- and B-unit and was created based on technical notes by GMV (GMV, 2022b). It consists of six surfaces describing the body of the satellite and two surfaces (front and back) for the solar panel. The macromodel of S6A is based on the technical documents of ESA (ESA, 2021). From this, a total of 10 surfaces were derived, eight for the body of the satellite and two describing the Advanved Microwave Receiver (AMR).

2.2. On DORIS time bias estimation

In order to take care of a possible DORIS time bias, we estimate a SLR-derived time bias, which is then applied to the DORIS data. For this purpose, in a first step a DORIS-SLR combined orbit is generated to perform data screening. After that the SLR observations are downweighted, so that the resulting orbit follows the DORIS time system. This orbit is then kept fixed and only a time bias value is estimated for the SLR observations. Finally this value is applied to the DORIS observations with a reversed sign to bring the DORIS observations as close as possible to the SLR time system. The respective estimates obtained are shown in Fig. 1 for all three satellites. The three missions show similar values among themselves and also the same structure over time with a slight increase of the difference. The average value for S3A is -0.63 ± 0.54 μs, for S3B -0.34 ± 0.56 μs and for S6A about -0.75 ± 0.65 μs. Translated into changes of the orbit, this corresponds to a mean transversal bias of 3–4 mm. Compared to values seen in the T2L2 and the analysis by Exertier et al. (2017) these inter technique time biases appear at a quite low level, that perhaps we have to be concerned about time consistency of all the techniques, not just DORIS w.r.t. SLR.

2.3. On the overall POD RMS of fit assessment

In order to validate the orbit accuracy, technique-specific RMS values for dedicated key parameters as well as SLR-derived RMS values are given in Table 4. Except in the DORIS with SLR combined approach, SLR is used but downweighted as an independent technique for validation. Global RMS values for SLR, either as a contribution in the combined case with DORIS, or purely as a validation technique, are typically below 1 cm, which is also comparable to those values achieved with GPS-derived orbits. The RMS values of DORIS measurement residuals are around 0.4 mm/s for all cases, which is at the same order of magnitude as those obtained by other groups (Capdeville and Lemoine, 2019; Peter et al., 2018). No variation over time can be observed in mean, RMS, standard deviation, and number of observations per arc for the three satellites. For a more detailed analysis of the DORIS residuals, Table 5 shows stations whose RMS values are above 0.5 mm/s. These are conspicuously above the mean residual distribution over all stations. Some of the stations are located in the South Atlantic Anomaly (SAA) region (marked with a *), which explains the higher RMS values. Whereas Grasse and Wettzell are stations with shifted beacon frequencies. Further investigations for an optimal solution in this case are ongoing. The influence of the SAA on satellites and the effect on DORIS observations for POD has been studied for several satellites in recent years. Schrama (2018) studied this effect for Cryosat-2 and saw the SAA effect also in the median of the residuals in the glo-

Table 3
Parameterization and models used for technique-wise precise orbit determination. T = transverse, N = normal.

	DORIS w/ SLR & DORIS	GPS	Reference
General			
Software	EPOS-OC (v6.74)	idem	(Zhu et al., 2004)
Arc-length	7 days	Const.: 30 h (21:00–03:00) LEO: 28 h (22:00–02:00)	
Dynamic model			
a priori gravity field	GOCO06s 120x120	idem	(Kvas et al., 2021)
	time variable120x120	idem	
Ocean pole tide	Desai30x30	idem	(Desai, 2002)
Ocean tide model	FES2014100x100	idem	(Lyard et al., 2021)
AOD	AOD1B RL06180x180	idem	(Dobslaw et al., 2017)
Atmosphere	MSISE-90	idem	(Hedin, 1991)
Atmospheric tide	BB2003	idem	(Biancale and Bode, 2006)
Earth tide	Wahr model	idem	(Wahr, 1981))
	IERS Conventions 2010	idem	(Petit and Luzum, 2010)
Albedo w/ IR	According to Heurtel	idem	
Satellitemodel	Macromodel	Macromodel	S6A: (ESA, 2021)
Geometric model			
EOP	IERS C04 14	idem	(Bizouard et al., 2018))
Ephemeris	DE430	idem	(Folkner et al., 2014)
Station coordinates	DPOD 2014 v. 5.5		(Moreaux et al., 2019)
	SLRF 2014 v. 200428		(ILRS, 2020)
		IGS2014 v. 22:180:15726	(Johnston et al., 2017)
Post-Seismic Deformation	ITRF2014	idem	(Altamimi et al., 2016)
Mean pole	linear mean pole	idem	(Ries, 2017)
Moon	FERRARI77	idem	(Ferrari, 1977)
Satellite configuration			
Attitude	Quaternions	idem	GMV
Center of mass	variable with input from FOS	idem	(CNES, 2022a)
Observations			
	SLR measurements DORIS integrated doppler count	GPS measurements	
Elevation angle cut-off	DORIS: 10 deg. SLR: 10 deg.	LEO: 0 deg. Ground: 20 deg.	
Downweighting law	None	None	
Obs. correction models			
Frequency bias and drift	once per sta. and pass estimated		
Optical phase map	Applied for SLR		
PCV+CPV-map		GFZ in-flight calibration	
Phase center windup		applied	
Range bias	one global biasestimated		
Time bias	estimated per arc		
Troposphere model	DORIS: VMF-1 SLR: MP 2004	GPS (ground): VMF-1	(Boehm et al., 2006) (Mendes and Pavlis, 2004)
Troposphere bias	once per sta. and pass estimated		
Parameterization			
Atmospheric drag	1 per 3 h	1 per 6 h	
Albedo w/ IR	1 linear scaling per arc estimated	fixed to 1.0	
Empirical acc.	1/rev cos,sin every 48 h in T and N direction	1/rev cos,sin every 75' in T and N direction	
Solar radiation	1/day	1/arc	
Ambiguities		estimated - float	

bal distribution. We have performed a similar investigation for the three Sentinel satellites. Fig. 2 shows the global distribution of the median of binned DORIS residuals. The geographical distribution shows, that the effect of the SAA is clearly visible for the three satellites. For S3B this effect appears to be smaller. Compared to the two Sentinel-3 satellites the SAA influence on the higher orbiting S6A satellite (1336 km instead of 797 km) appears somewhat more distributed also over Ascension (South Atlantic Ocean) with the strongest effect over Arequipa (Peru). Both S3A and S3B also show a slight pattern near the Syowa station at the South Pole and even less in the Southeast Asian region. Syowa has been reporting a Beacon failure since the beginning of 2021, which may be a reason for the increased RMS values. At this point, it sould be noted that for all three satellites, the GNSS receiver is connected to the DORIS USO, and can provide independent clock solutions to model the USO behavior. Štěpánek

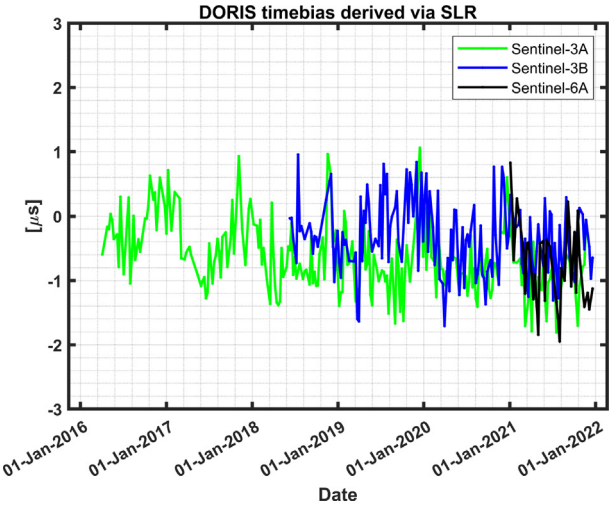

Fig. 1. Estimated DORIS time bias derived via SLR.

et al. (2021) made a demonstration of how these clock solutions could be used to model these SAA induced perturbations of the DORIS USO's on S3A and S3B.

3. Technique-wise orbit comparison

3.1. Orbit comparisons

The orbits for the three satellites have been created in three variants. In the first variant, SLR and DORIS observations were processed together, with a weighting derived from their global RMS values. The second version is based on DORIS observations only, SLR was used for validation purposes only. The time bias, which was previously calculated using the SLR observations, is applied to the DORIS observations for each week in this version. The third version was generated from January 2021 onwards, and is based on GPS observations alone. SLR is used here for validation only. The CPOD combination solution is used as the reference solution for the following comparisons (GMV, 2022a). Being the combination of all contributing partners, it is assumed to be the most accurate, i.e. that the residual errors are minimal, and that the absolute position accuracy is highest. Table 6 lists the statistics of the orbit comparisons of the three different variants of the POD for the three satellites. The SLR RMS values here refer to the internal validation, where one range bias per station per arc was estimated. In the comparison of the techniques among each other, the systematic deviations compared to the reference solution with the GPS determined orbits are minimal with values in the mm range. The two variants with DORIS-only and in combination with SLR show very similar results. For S3A there is a radial bias of 2.8 mm. The mean deviations in normal direction are negligible and agree well with the values of the GPS solution. For S3B no clear systematic deviations can be detected. For S3A and S3B the remaining deviation after correcting the DORIS time bias (compare Section 2.2) sizes near 2 mm in transverse direction. For Sentinel-6A, the largest differences appear in the transverse direction. They are near 1 cm. With 1.7 mm, that value is much smaller in the GPS-based solution. In the normal direction, the deviations of the DORIS-only and DORIS with SLR solutions are at a level of 6 mm. The corresponding score for the GPS-only solution is remarkably smaller with 3 mm. In the radial direction, the GPS-based solution is closest to the reference solution, but the other two also agree relatively well with a value of about 1 mm. A comparison of the RMS values shows similar values below the cm for all three variants in the radial direction. The values for GPS are slightly better for Sentinel-6A. The orbits based on GPS observations show up to 50% lower RMS values, especially in transverse and normal direction. In the transverse direction, this can be seen especially for Sentinel-6A. In general comparison, the RMS values in transverse and normal direction for DORIS based orbits with typical values below 2 cm are on a good level, which is comparable to

Table 5
Stations with mean DORIS residuals over 0.5 mm/s. Values given in mm/s. Stations marked with a * are located in or near the SAA region.

Code	Name	S3A	S3B	S6A
CADB	CACHOEIRA-PAULISTA*	0.54	0.50	0.46
GR4B	GRASSE	0.56	0.57	0.51
KRWB	KOUROU*	0.49	0.50	0.47
LAOB	LE-LAMENTIN*	0.51	0.52	0.49
WEUC	WETTZELL	0.52	0.55	0.55

Table 4
Post fit residuals and number of observations for the three satellites in the combined SLR with DORIS, DORIS-only with SLR as validation and GPS-only with SLR as validation. v stands for validation. Time span is the full mission duration until Dec-2021, only cases marked with * have a time span from Jan-2021 to Dec-2021.

		Sentinel-3A			Sentinel-3B			Sentinel-6A		
		RMS	Mean	No. Obs.	RMS	Mean	No. Obs.	RMS	Mean	No. Obs.
SLR	[cm]	0.75	−0.01	271,387	0.79	0	154,355	0.69	−0.01	53,404
DORIS	[mm/s]	0.41	0	16,212,601	0.42	0	9,820,344	0.38	0	3,963,499
SLR^v	[cm]	0.97	0	271,387	1.01	0	154,355	0.86	0.02	53,404
DORIS	[mm/s]	0.40	0	16,212,601	0.42	0	9,820,344	0.38	0	3,963,499
SLR^v*	[cm]	1.27	0	50,098	1.25	0	51,372	1.24	0	67,254
GPS-Code*	[cm]	38.9	−0.03	14,812,714	37.5	−0.13	15,348,416	85.8	0.06	15,566,084
GPS-Phase*	[mm]	3.1	0	14,812,714	3.2	0	15,348,416	4.0	0	15,566,084

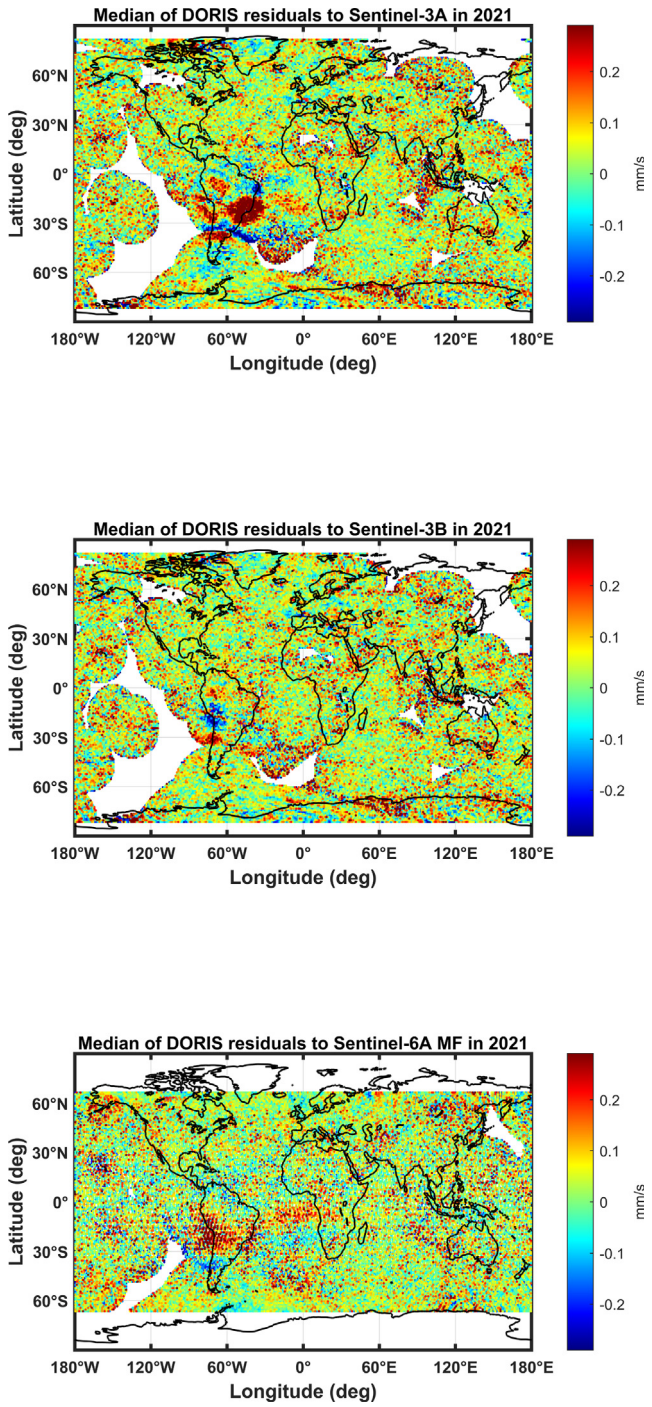

Fig. 2. Median of DORIS residuals for the three satellites in 2021. The SAA region is prominent visible for all satellites.

those of other groups (GMV, 2022a; Capdeville and Lemoine, 2019; Peter et al., 2018). In the comparison of the satellites, S6A in the transverse and normal directions especially stands out. Apart from the systematic deviation in transverse direction of about 1 cm, which is not to be noted for GPS, all three orbit variants show higher deviations in the normal direction that do both of the Sentinel-3 satellites. A reason for this could be a possibly necessary adjustment of the macromodel and dynamic modeling, a discrepancy of the inter technique reference points, or in the transverse direction also an actual higher than adjusted DORIS time bias. It is presently not possible to deal with self-shadowing effects between surfaces. This might be necessary for Sentinel-6A due to its design (See also Montenbruck et al. (2021)). Depending on the beta angle, the extended solar panels cause a part of the satellite body to be shadowed, which changes the directly irradiated area. Lack of modeling of this effect can lead to errors. A global comparison of the DORIS orbit solutions with the reference solutions in the radial direction is shown in Fig. 3. We show radial differences since the three missions are altimetry missions. For altimetry applications, the radial component is of essential interest since it has a direct impact on the information derived from measurements. For both Sentinel-3 satellites, the global pattern of the deviation is quite similar and shows an East–West structure. Radial positive differences occur here in Western longitudes. Contrary to this, the comparison for S6A shows an inverse structure. Here positive differences are visible in Eastern longitudes. This structure can also be found in the orbit comparison by GMV for the contributors to the combined orbit solutions for the DORIS based solution by CLS (This solution is named GRG in (GMV, 2022a)). Compared to the combined orbit solution, the CLS solution shows the same East–West structure for the Sentinel-3 satellites and the opposite structure for Sentinel-6A as found here for the GFZ DORIS+SLR solution. This indicates that this is either a DORIS-specific effect or an effect due to the dynamic modeling and not coming from the POD software (CLS uses GINS/DYNAMO, GFZ uses EPOS-OC).

3.2. Empirical accelerations

In the dyanamic orbit determination, we estimate empirical acceleration, cosine and sine, respectively, in transversal and normal direction. These estimated accelerations are shown in Fig. 4 for S3A and Fig. 5 for S6A. The unit of the parameters is shown in $[nm/s^2]$, and next to it the corresponding power spectrum. The weighted mean of the accelerations and their standard deviations are given in the title of the respective figures. In each case, the bottom left figure shows the beta angle over time. The beta angle of S3A shows an annual and semi-annual period with a variability of approximately 12 degree. Unmodeled perturbation forces are efficiently absorbed by the sine term in transversal direction, to a smaller extent also by the cosine term and the sine term in normal direction. The least periodicity can be found in the cosine term in normal direction, with annual values in the power spectrum even one order of magnitude smaller. Compared to the values of S3A, the empirical accelerations of S6A show significantly larger amplitudes. The periodicity of the beta angle of S6A is about 118 days. Compared to S3A, this angle varies over a much larger range of ±80degrees. This period can be

Table 6
Orbital comparison against CPOD combined reference solution. (GMV, 2022a).

	Radial		Transverse		Normal	
	Mean [cm]	RMS [cm]	Mean [cm]	RMS [cm]	Mean [cm]	RMS [cm]
Sentinel-3A						
DORIS w/ SLR	0.28	0.82	−0.26	1.85	−0.08	1.49
DORIS	0.28	0.82	−0.23	1.88	−0.08	1.48
GPS	−0.03	0.75	0.07	1.21	0.02	0.74
Sentinel-3B						
DORIS w/ SLR	0.10	0.80	0.07	1.90	0.09	1.61
DORIS	0.10	0.80	0.14	1.96	0.09	1.65
GPS	−0.09	0.74	0.02	1.33	0.05	0.69
Sentinel-6A						
DORIS w/ SLR	0.13	0.74	−0.99	2.12	−0.66	1.51
DORIS	0.13	0.75	−1.15	2.24	−0.65	1.55
GPS	−0.04	0.60	−0.17	1.28	−0.33	1.01

found primarily in the sine and cosine accelerations in transversal direction. Compared to those of S3A, the values for S6A are larger. In the normal accelerations, periodicities around 95 and 275 days are more prominent. The spectra also show an increase in the higher frequency range, which could correspond to the orbital repeat cycle of 10 days.

In addition to the empirical accelerations, the dynamical parameterization also estimates scaling factors for the radiation pressure (CR), the atmospheric drag (CD), and the Earth Albedo including infrared radiation (Albedo+IR). For S3A, CR and CD show mainly an annual periodicity, which fits the period of the beta angle. For S6A CR, CD and Albedo+IR show a periodicity of 85 days. A comparison of the statistics of these values is given in Table 7 and shows a good agreement of the values for S3A and S3B, whereby they show a lower standard deviation than those of S6A. Especially the CD value for S6A is striking with a significantly increased standard deviation and a weighted mean of −1.950. This is most likely due to the macromodel used and the fact that currently no self-shadowing of surfaces is implemented in EPOS-OC. Thus, the antenna in the macromodel probably leads to this effect. The shadow function, as well as an adapted macromodel, is currently under development. At this point and also in context of Section 3.3, the course of the estimated Albedo+IR coefficient is worth mentioning. This coefficient shows for S3A and S3B very stable values with a small standard deviation, but this value drifts over time. The standard deviation of this value is significantly larger for S6A (see Fig. 6).

3.3. DORIS antenna reference point estimation

Motivated by a +10 mm center-of-mass correction for S3A seen by Montenbruck et al. (2017) and adjusted DORIS reference point values communicated in Cerri et al. (2021) (hereafter referred to as IDS values), we estimate the ionosphere free DORIS reference point with respect to the global station network, to see if we can replicate these estimates. At this point it should be noted that the estimation of reference points of observation techniques on a satellite strongly depends on the modeling of the non-gravitational forces. Effects that are not modeled optimally can lead to direct influences here. By combining several observation techniques this effect can be reduced. Therefore, two versions were created, one based only on DORIS and one based on a combination of all available observation techniques. For the first version, we estimate for the reference point coordinates based on the weekly arcs and generated weekly normal equations. After these weekly normal equations were each inverted separately to obtain estimated values with weekly temporal resolution, the mission duration was divided into several stages based on a time series of center-of-mass correction epochs where the satellite did not undergo a center-of-mass correction in normal and transverse direction. Within these stages, the respective normal equations were accumulated to obtain a highly accurate estimate for that epoch. The values for this are listed in Table 8 with their respective standard deviation. The weekly values, as well as the subdivision of the individual stages and the corresponding center-of-mass corrections are shown in Fig. 7. The estimated values of the reference point in the normal and transverse directions are stable over time and slightly less noisy for S3A and S3B. In the radial direction, S3A stands out, where the values start around 0 at the beginning of the mission and increase by about 1.5 cm over the years. This corresponds approximately to the transverse center-of-mass variations as provided by CNES (2022a) over this period (See Fig. 7 left graphics). For S3B, this effect is similar, and shows an increase over the approximately 4 years. The drifts are for both, S3A and S3B, approximately 3 mm per year. Comparing the corrections of S3B for the same period of S3A shows that for both missions the corrections are stable in the period from January 2019 to about January 2021. What stands out here is that before this period and after this period the same trends can be seen for both satellites. For both satellites,the increase in corrections in the radial direction beginning of 2021 sizes about 5 mm. Further investigations on this are also described in Section 4, to which reference is made here. After this increase, the values remain more stable at this level. For S6A, the corrections

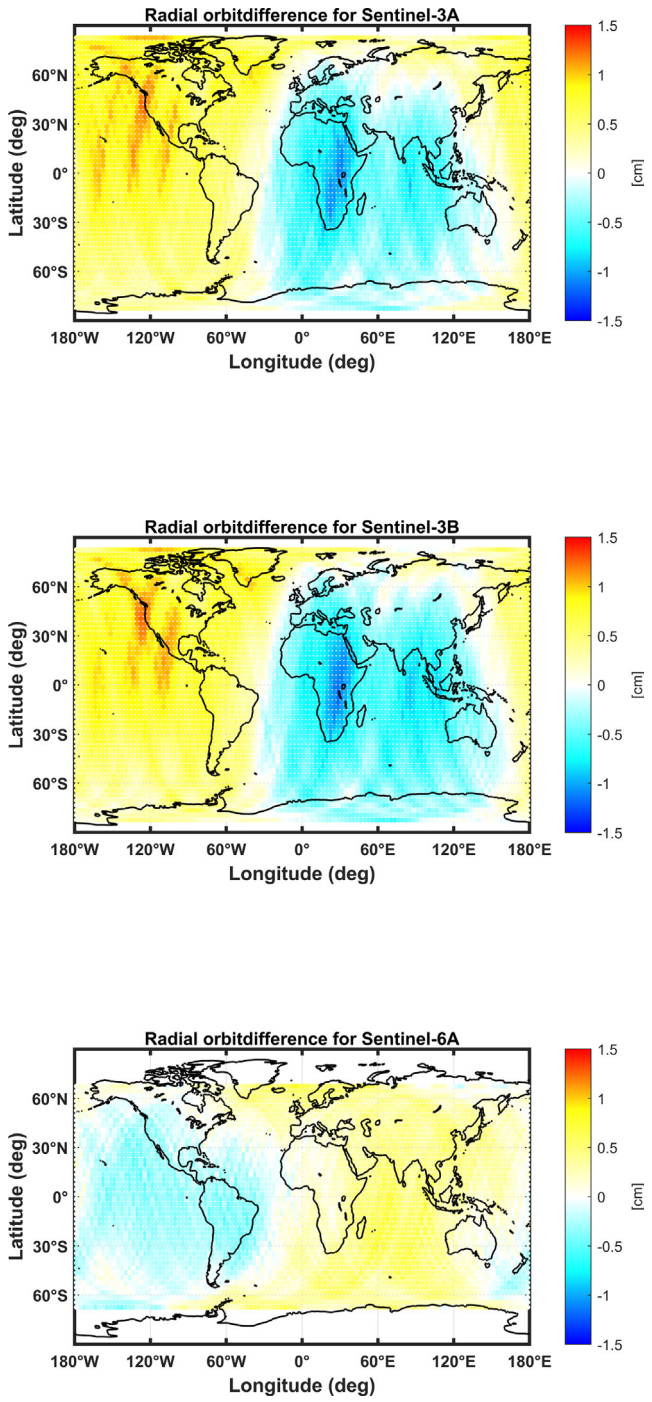

Fig. 3. Orbit comparison for the three Sentinel satellites, DORIS+SLR orbit compared to CPOD combined orbit solution in the year 2021.

are stable over the present mission time. However, during the period of estimation of S6A, the other two satellites are also stable at their increased levels. Comparing the values estimated by IDS with the manufacturer's values, we see a difference of −10 mm in radial direction for both Sentinel-3 satellites and +16 mm correction in normal direction for S3A and +10 mm for S3B. The estimates of the individual stages for S3A and S3B in radial direction vary as mentioned over the evaluated mission period. In the stable period from January 2019 to January 2021, we see a +8–9 mm correction in the radial direction for S3A (Stage 3 and 4) and −4 mm for S3B (Stage 2). In both cases, however, we see significant differences from the IDS values. In the transverse direction, the IDS values agree with the manufacturer's specifications, and the estimation also shows no significant corrections over the different stages. However, a possible position error in the transverse direction can hardly be distinguished from a time bias, whereby possible corrections would also result in the corrected time bias. In the normal direction, we see a correction of +2 mm for S3A, and only +1 mm for S3B. The values estimated by IDS cannot be seen in this step. Also the center-of-mass correction in normal direction for S3A according to (Montenbruck et al., 2017) cannot be reflected with this approach. Whereby it is also worth mentioning that no systematic deviation in normal direction could be seen in the orbit comparison for both satellites.

For Sentinel-6A, the corrections in transverse direction are about −3–4 mm compared to the manufacturer's specifications (The transversal inter-technique orbital difference seen in Section 2.3 for S6A sizes about 10 mm). The IDS reference point values do not differ from the manufacturer's specifications. The estimates in radial and normal direction for stage 1 and 2 show differences compared to the manufacturer's values of 0 to +2 mm.

To go one step further we validate this correction values with multiple techniques available. A period of three weeks in the time span of the last stage (gpsweek 2178 to 2180 - Nov. 2021) was chosen and three technique, i.e. DORIS, GNSS (Galileo and GPS for S6A) and SLR, combined arcs were generated. The GNSS approach including also Galileo, follows the exact same approach as the GPS only case, besides the fact, that it also includes Galileo observations and a inter system bias is estimated. For highest accuracy we used single receiver cycle slip fixed data (Michalak et al., 2017; Schreiner et al., 2021). In this combined arc, we use an arc length of 24 h (00:00 h UT to 00:00 h UT), we estimate the reference point of the DORIS, GNSS antenna and SLR retro reflector simultaneously and set up normal equations. The daily normal equations are subsequently stacked over the whole timeperiod and solved. The hereby derived values are also listed in Table 8.

If we first look at the correction value for S6A in radial direction, the correction value for DORIS increases slightly and shows +3 mm deviation from the manufacturer's value, but is close to the significance limit. SLR shows no significant difference, for the GNSS position it is −3 mm. In transverse direction, the multi-technique estimation shows no differences to the manufacturer values for all techniques. The +2 mm difference seen for DORIS in normal direction in the single technique approach also shows up here, but not significantly, and for SLR even −6 mm arise. For the GPS referece point of the two Sentinel-3 satellites, we see corrections to the a priori values of 1–3 mm in the transverse and normal directions and 4 to 5

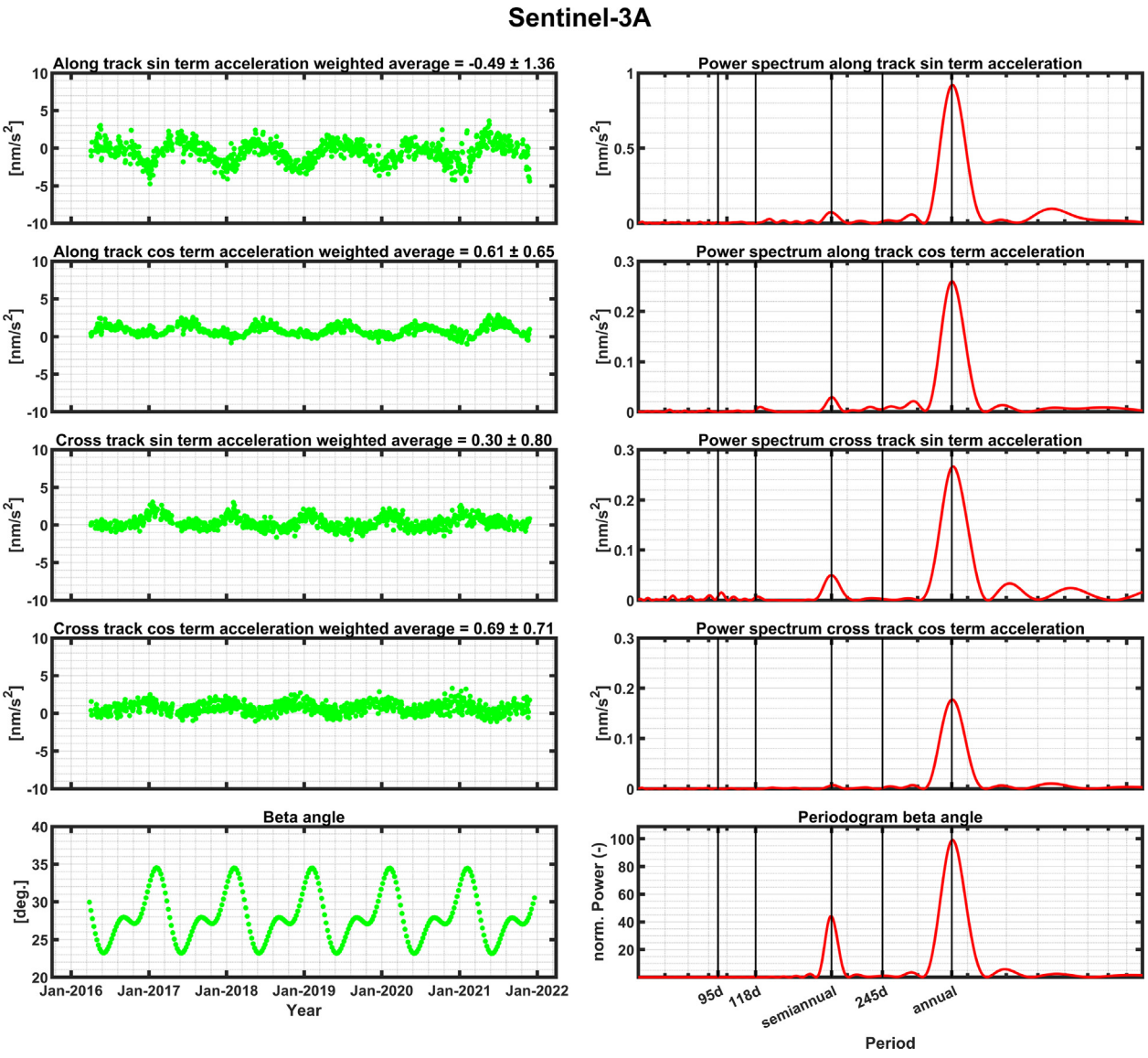

Fig. 4. Estimated empirical accelerations for Sentinel-3A on the left, appropriate power spectrum of the acceleration on the right. The bottom figure shows the beta angle. The weighted average of the acceleration and it's standard deviation is given in the title of the respective figure.

mm difference in the radial direction for each of the GPS antennas in the multi technique estimate. If we apply the estimated radial corrections for the three satellites to the GPS-PCO values, that would bring the GPS-PCO values of the three satellites together to one value. S3A and S3B: 68 mm + 4 mm = 72 mm and for S6A 75 mm - 3 mm = 72 mm. For the laser retroreflector, no major differences from the a priori values used can be seen; the differences are between 0 and 3 mm. The differences of the DORIS antennas show no difference in transversal direction. However, in normal direction the correction is +17 mm for S3A and +8 mm for S3B. These values fit very well to those published by Cerri et al. (2021) and also show for all techniques +8–9 mm difference in normal direction between the two satellites, comparable to the +10 mm CoM deviation for S3A according to Montenbruck et al. (2017). Furthermore, the DORIS reference points show an additional offset in normal direction of +8–9 mm. The strongest corrections can be seen for both satellites in the radial direction. This is +25 mm for S3A and +8 mm for S3B. These values are thus even larger than those estimated with DORIS alone. Adjusted values by IDS are −10 mm in the other direction, starting from the manufacturer's value. Part of the differences for S3A can also be seen in Section 4, to which reference is made here.

4. DORIS based local reference frame determination

To derive weekly reference frame solutions we estimate station positions as well as daily pole coordinates and LOD. We validate the computed station coordinates using the reference frame determining parameters (translation, rotation, and scale), through a Helmert transformation compared to the a priori station network. The scale is con-

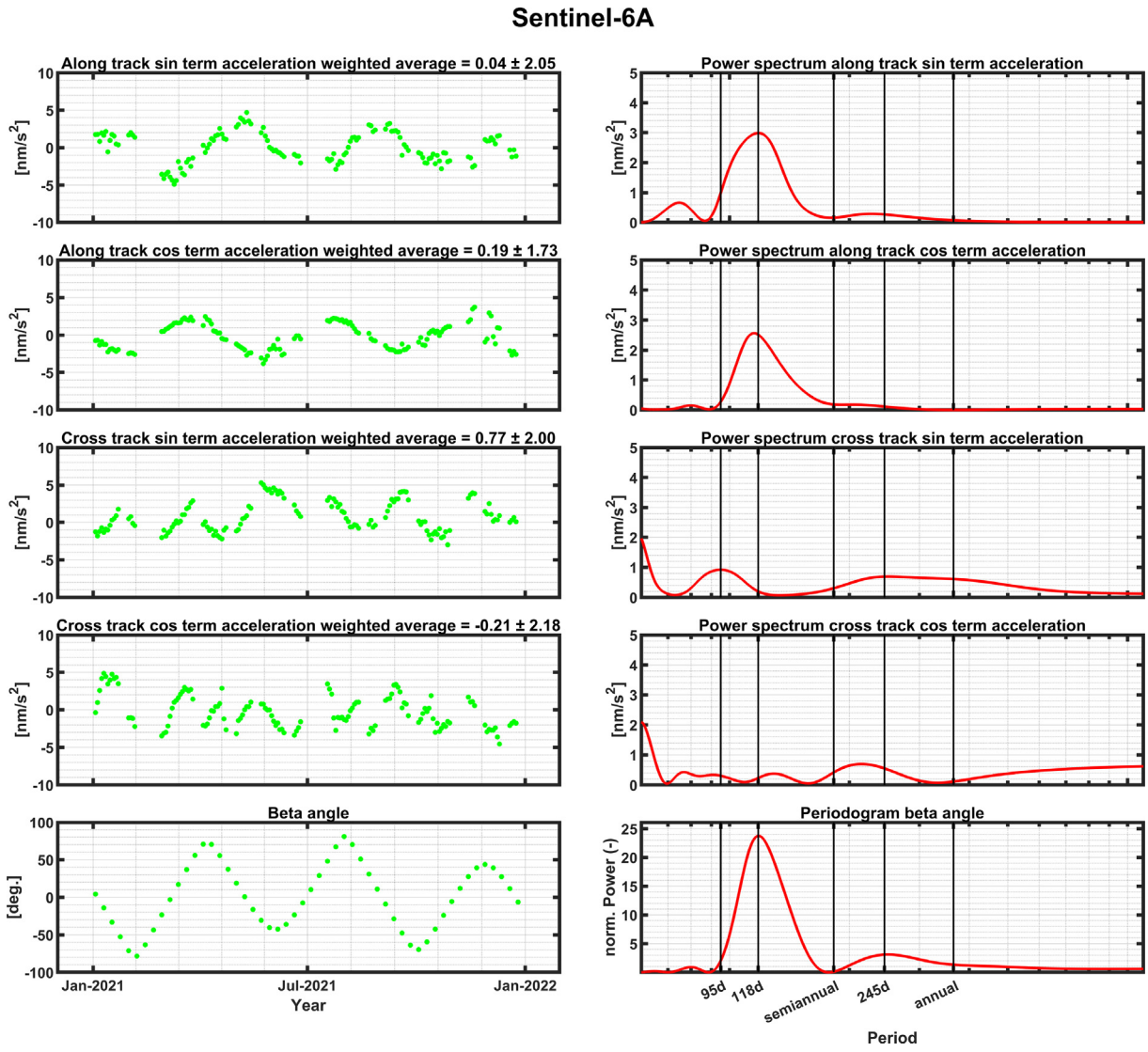

Fig. 5. Estimated empirical accelerations for Sentinel-6A on the left, appropriate power spectrum of the acceleration on the right. The bottom figure shows the beta angle. The weighted average of the acceleration and it's standard deviation is given in the title of the respective figure.

Table 7
Statistics of the scaling factors for SRP (CR), Drag (CD) and Albedo+IR (CAI). Weighted average (wav.) and trend per decade (t.p.d.).

	S3A	S3B	S6A
CR			
w.av.	0.998 ± 0.024	0.987 ± 0.023	0.979 ± 0.064
t.p.d.	0.004 ± 0.004	−0.003 ± 0.007	0.509 ± 0.135
CD			
w.av.	0.816 ± 0.251	0.815 ± 0.260	−1.950 ± 1.955
t.p.d.	−0.242 ± 0.013	0.092 ± 0.029	1.486 ± 1.593
CAI			
w.av.	0.995 ± 0.003	0.996 ± 0.002	0.948 ± 0.056
t.p.d.	−0.009 ± 0.001	−0.010 ± 0.001	−0.082 ± 0.234

verted to mm by multiplying it by the mean radius of the Earth. Shown Helmert parameters always refer to the entirety of the station network, only stations with a 3-D position deviation above 0.5 m are excluded. Calculated mean values and standard deviations of these parameters

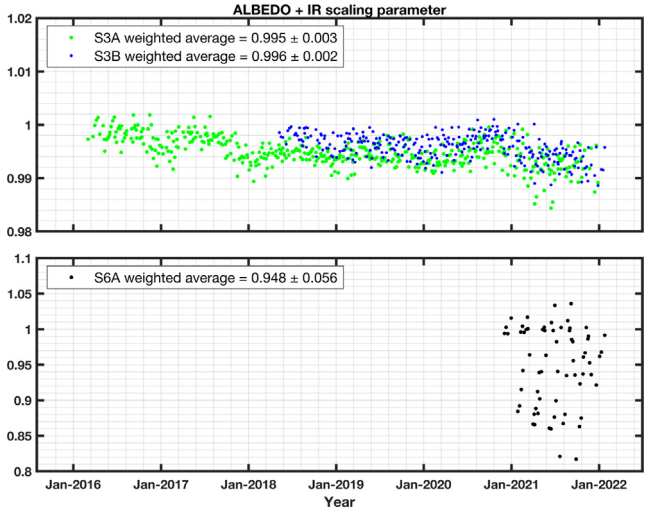

Fig. 6. Estimated scaling parameter for Earth Albedo+IR.

Table 8
Estimated DORIS ionosphere free reference point coordinates in comparison to manufacturer values and values published by Cerri et al. (2021). Values marked with * were used in the POD process. The 1.0 cm in normal direction for the Sentinel-3A manufacture value according to Montenbruck et al. (2017).

	Radial [cm]	Transversal [cm]	Normal [cm]
Sentinel-3A	-Z (S/C)	-X (S/C)	-Y (S/C)
DORIS (Manufacturer)*	−107.3	−156.9	7.3
DORIS (IDS)	−108.3	−156.9	8.9
GPS-1 (Manufacturer)	79.4	−288.1	−20.0
GPS-1 (CPOD)*	79.4	−288.1	−19.0
SLR (Manufacturer)	−80.1	−113.4	63.8
SLR (CPOD)*	−80.1	−113.4	64.8
DORIS (est. stage 1)	−107.2 ± 0.02	−156.8 ± 0.14	7.5 ± 0.02
DORIS (est. stage 2)	−106.8 ± 0.02	−156.8 ± 0.13	7.5 ± 0.02
DORIS (est. stage 3)	−106.5 ± 0.03	−156.8 ± 0.18	7.5 ± 0.03
DORIS (est. stage 4)	−106.4 ± 0.02	−156.8 ± 0.15	7.4 ± 0.03
DORIS (est. stage 5)	**−105.8 ± 0.03**	**−156.8 ± 0.16**	**7.5 ± 0.03**
DORIS (comb. appr.)	**−104.8 ± 0.11**	**−156.9 ± 0.19**	**9.0 ± 0.15**
GPS-1 (comb. appr.)	79.9 ± 0.01	−287.9 ± 0.13	−19.3 ± 0.01
SLR (comb. appr.)	−79.8 ± 0.12	−113.4 ± 0.13	64.7 ± 0.01
Sentinel-3B	-Z (S/C)	-X (S/C)	-Y (S/C)
DORIS (Manufacturer)*	−107.3	−156.9	7.3
DORIS (IDS)	−108.3	−156.9	8.3
GPS-1 (Manufacturer)*	79.4	−288.1	−20.0
SLR (Manufacturer)*	−80.1	−113.4	63.8
DORIS (est. stage 1)	−108.0 ± 0.04	−156.8 ± 0.27	7.4 ± 0.05
DORIS (est. stage 2)	−107.7 ± 0.02	−156.8 ± 0.12	7.4 ± 0.02
DORIS (est. stage 3)	**−107.3 ± 0.02**	**−156.8 ± 0.15**	**7.4 ± 0.03**
DORIS (comb. appr.)	**−106.5 ± 0.11**	**−156.9 ± 0.20**	**8.1 ± 0.16**
GPS-1 (comb. appr.)	79.8 ± 0.01	−287.9 ± 0.14	−20.1 ± 0.01
SLR (comb. appr.)	−80.1 ± 0.13	−113.2 ± 0.14	63.9 ± 0.01
Sentinel-6A	-Z (S/C)	-X (S/C)	Y (S/C)
DORIS (Manufacturer)*	−100.4	−162.5	40.0
DORIS (IDS)	−100.4	−162.5	40.0
GNSS-1 (Manufacturer)*	108.0	−247.5	0.0
SLR (Manufacturer)*	−66.5	−162.5	−40.1
DORIS (est. stage 1)	−100.3 ± 0.07	−162.8 ± 0.25	40.0 ± 0.07
DORIS (est. stage 2)	**−100.4 ± 0.04**	**−162.9 ± 0.17**	**40.2 ± 0.05**
DORIS (comb. appr.)	**−100.1 ± 0.19**	**−162.6 ± 0.26**	**40.2 ± 0.24**
GNSS-1 (comb. appr.)	107.7 ± 0.02	−247.5 ± 0.12	−0.0 ± 0.05
SLR (comb. appr.)	−66.4 ± 0.17	−162.5 ± 0.12	−40.7 ± 0.07

are not subject to any further filtering or similar (See Table 9). The calculated Earth orientation parameters listed in Table 10 were in all cases first filtered with a 2.576σ filter to exclude coarse outliers. For this purpose three different solutions were generated, first a nearly complete free solution, second a solution using a no-net-rotation condition and third a combined solution with a no-net-rotation condition applied. (see Table 11).

In the first version, we use only a weak constraint of 1 m for station coordinates and EOPs. If we solve the resulting normal equations, we see major scatter in X- and Y-pole coordinates in comparison with a priori (EOP 14 C04) with standard deviation values of 1.5–3 cm. Noticeable in the derived pole coordinates is also a jumping behavior, whereby no systematic pattern in this behavior can be recognized. The values for LOD are better, showing no mean deviation, and lower standard deviation with values of 1–2.5 cm in the datum-free case. A look at the Helmert parameters shows all three rotations to be higher with values up to 1 cm. For this reason we apply only a no-net-rotation (NNR) constraint in the second version. For the strength of the conditions we use an equivalent of 1 mm, following the recommendation by Altamimi (2002), on a dedicated subset of stations. The sub-network of stations for the NNR condition is found through an iterative process. The NNR condition is first applied to all stations in the solution. Then the 3-D station coordinate differences to a priori are calculated and the stations are one-by-one excluded from the NNR-condition, if they do not fulfill the condition $3\sqrt{3}cm > \sqrt{\Delta x^2 + \Delta y^2 + \Delta z^2}$. In this way the observed rotations can efficiently be reduced to a minimum (Compare values in Table 9 for "Free" with "With NNR"). The values of the translations and scale remain about the same, only Sentinel-3B and Sentinel-6A show a slight change in the Z-translation, which is not significant. The rotations of the whole station network (not only datum stations) show significant improvements, they are in the mean as well as the standard deviation now in the low mm range. This method can also significantly reduce the scatter of the polar coordinates by a factor of up to

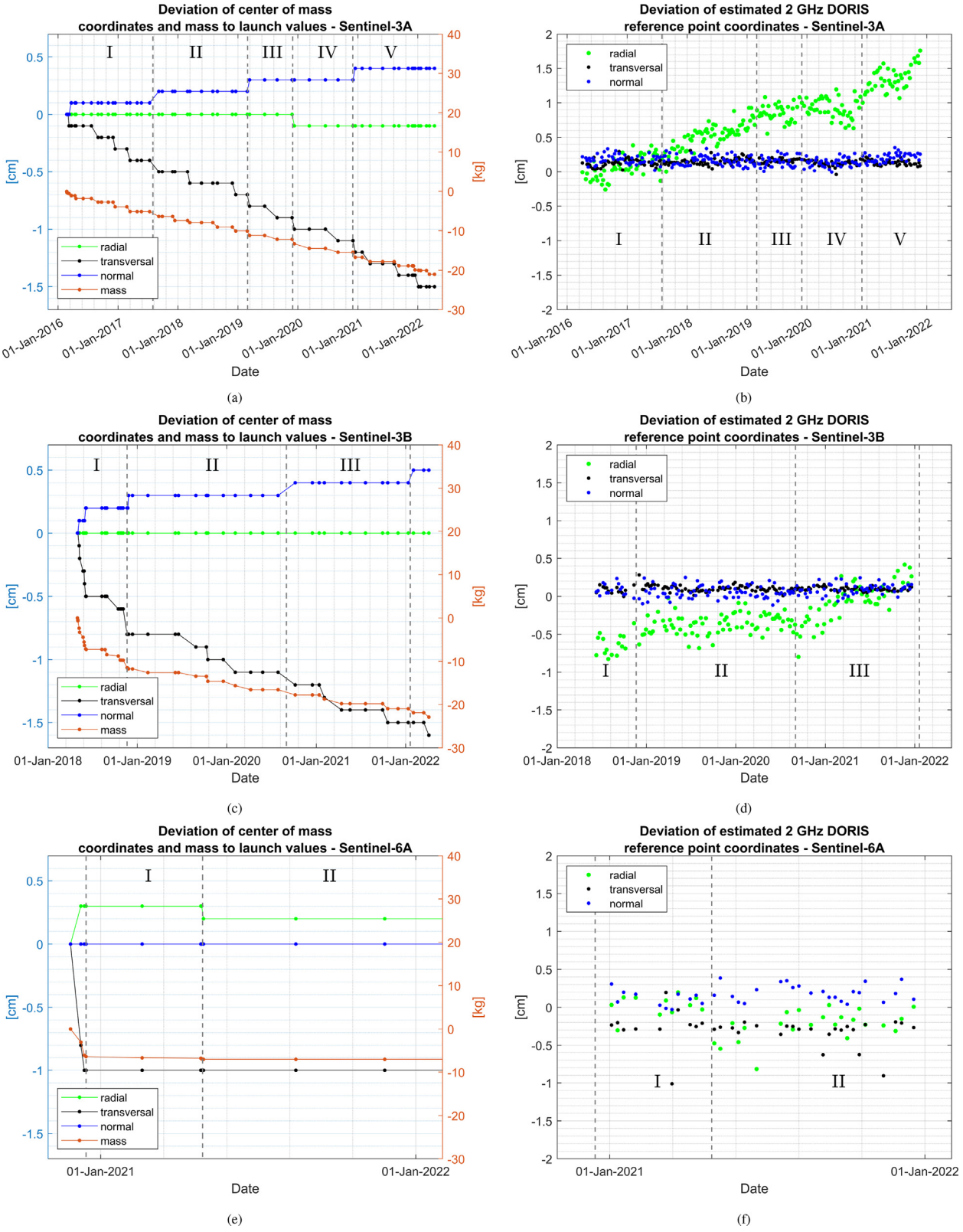

Fig. 7. The figures on the left show center-of-mass coordinates and mass variation over time in relation to manufacture launch values. The figures on the right show the estimated coordinate difference of the ionosphere free DORIS reference point. The areas marked with Latin numerals show individual stages where the satellite did not undergo a center-of-mass correction in normal and transverse direction. These stages were used for estimating one set of reference point coordinates over the whole epoch.

Table 9
Comparison of the derived Helmert parameters in comparison with a priori. Mean and standard deviation of weekly values.

	Tx [mm]	Ty [mm]	Tz [mm]	Rx [mm]	Ry [mm]	Rz [mm]	Scale [mm]
Free							
Sentinel-3A	3.01 ± 1.78	1.88 ± 2.48	1.92 ± 6.50	10.01 ± 32.35	3.27 ± 17.89	−6.52 ± 7.21	−4.93 ± 2.47
Sentinel-3B	4.92 ± 1.76	3.05 ± 2.17	−3.55 ± 7.01	4.30 ± 35.65	5.65 ± 20.61	−3.80 ± 9.77	−0.07 ± 1.55
Sentinel-6A	2.36 ± 2.84	−3.45 ± 2.90	0.00 ± 6.00	−9.91 ± 21.50	−1.40 ± 21.26	−7.80 ± 30.72	−0.26 ± 1.94
With NNR							
Sentinel-3A	3.02 ± 1.78	1.85 ± 2.47	1.29 ± 5.15	−1.82 ± 0.99	2.35 ± 1.72	−6.60 ± 1.45	−4.86 ± 2.47
Sentinel-3B	4.86 ± 1.78	3.07 ± 2.20	−0.05 ± 5.60	−2.40 ± 0.88	3.15 ± 1.95	−6.71 ± 1.32	−0.02 ± 1.50
Sentinel-6A	2.39 ± 2.81	−3.42 ± 2.92	−2.40 ± 5.59	−2.10 ± 1.58	5.35 ± 2.13	−9.16 ± 2.88	−0.33 ± 1.87
Combined	3.36 ± 1.75	1.80 ± 2.53	0.87 ± 3.94	−1.71 ± 1.00	2.59 ± 1.61	−6.57 ± 1.30	−2.61 ± 1.79

Table 10
Comparison of the derived EOPs with a priori values (EOP 14 C04). Weighted mean, standard deviation and yearly trend after applying a 2.576σ filter. Values for Sentinel-6A, especially those marked with * should be interpreted with caution, due to the short period of data.

	X-pole [μas]		Y-pole[μas]		LOD[μs]	
	Mean	Trend/a	Mean	Trend/a	Mean	Trend/a
Free						
Sentinel-3A	−44.68 ± 491.85	2.17	121.72 ± 828.73	62.05	0.06 ± 26.62	0.36
Sentinel-3B	131.73 ± 526.78	−3.52	−13.50 ± 884.75	86.53	−0.03 ± 40.44	2.55
Sentinel-6A	71.60 ± 632.27	−1163.13*	−379.14 ± 714.14	173.53*	0.01 ± 35.92	12.67*
With NNR						
Sentinel-3A	−77.40 ± 187.26	23.04	−140.88 ± 172.00	−2.32	0.03 ± 22.30	0.69
Sentinel-3B	8.64 ± 231.91	27.98	−180.19 ± 197.26	−2.18	0.00 ± 39.39	2.74
Sentinel-6A	172.96 ± 179.76	−104.62*	−177.95 ± 170.17	97.62*	0.02 ± 28.65	−1.88*
Combined	−15.64 ± 182.75	43.53	−148.24 ± 152.58	−7.15	0.00 ± 19.23	0.16

Table 11
Stations excluded from the NNR condition. (Number of arcs a station was observed with percentage of arcs the station is excluded).

Station		S3A		S3B		S6A	
Code	Name	No. arcs	Excluded [%]	No. arcs	Excluded [%]	No. arcs	Excluded [%]
BETB	BETIO	140	19.3	96	32.3	34	17.6
KEVC	KERGUELEN	114	27.2	31	83.9	0	0
SJUC	SAN JUAN	102	62.8	101	63.4	27	100
SOEB	SOCORRO ISLAND	25	92	0	0	0	0

5. The standard deviations of the polar coordinates are thus in the mm range, that for LOD shows no further improvement.

The pole coordinates show slight deviations on average from the a priori time series, although not significant. To check whether this method of evaluation is sensitive to a possible bias in the pole coordinates, a bias of 100[μas] was applied to the a priori time series and the processing was repeated. The pole coordinates determined here show a major part of the bias introduced. Thus, the introduced bias could not be fully removed.

Starting from the normal equations of the single satellite solutions, the third variant is a combined solution on normal equation level. Subsequently, a NNR condition was also applied to this solution. By the combination the Helmert parameters improve mostly in Z direction of the translation, here the standard deviation decreases by about 25%. The pole coordinates and LOD also show improvements by the combination, these are in the range of 10 to 20%. Transferred to Earth's surface the standard deviation of the derived pole coordinates of the combined solution sizes at around 6 mm for X- and 5 mm for Y-pole. The standard deviation for LOD is with values of about 9 mm comparable to those of the pole coordinates, whereby non of the values shows a statistically significant offset to a priori.

The derived trend is smallest for S3A and highest for S3B, but neither of these values is only close to a significant signal given the mission duration and standard deviation. The trend values for Sentinel-6A should be interpreted with caution, due to the shorter evaluation period of one year.

If we compare the values of "with NNR" for pole coordinates and Helmert parameters with values given in Moreaux et al. (2016) or Moreaux et al. (2023) for a combined DORIS solution, the single-satellite results obtained in this study show comparable standard deviations for translation and pole coordinates. The standard deviation obtained here for Tz is slightly lower.

The time series of translation and scale is shown in Fig. 8. Compared to Sentinel-3A, the scale for Sentinel-3B is slightly higher until 2020. One reason for this could be remaining minimal deviations of the radial component

of the DORIS antenna reference point. The value in radial direction is identical, but the estimated values show a deviation of about 12 mm in the overlapping stable period from about January 2019 to January 2021 (compare also Section 3). Sentinel-6A agrees quite well with S3B in terms of scale with values near 0 mm. The 8 mm radial correction of the multi technique estimate for S3B cannot be confirmed based on the scale. Furthermore, S3A shows a noticeable negative trend in scale over time. This was also noticed in the estimation of the radial reference points and the estimated scaling factors for the Albedo+IR. To exclude the Albedo+IR model as a possible reason for this, a version without any Albedo+IR modeling was created. The missing Albedo+IR modeling could be compensated by the used parameterization of empirical accelerations. The results for the radial reference point estimation remained identical, as well as the scale. A further attempt was also made to exclude DORIS stations that have been added to the network or have undergone a change from the processing, but this did not change this effect as well. To also exclude that this effect comes from the distribution of the DORIS station network, the center of the network in latitude was evaluated, unweighted, and weighted based on the accepted observations (See Fig. 9), whereby no correlations with the scale could be seen. Therefore the reason for this is still uncertain at the moment, since the orbit comparisons are not informative. The scale of the combined solution is showing more stability with the launch of S3B. With the addition of S6A, this is increasingly dominated by S3B and S6A, which also match well in the single-satellite solutions.

To further evaluate the station coordinates in more detail, the correction of the weekly station position in north, east and height component was evaluated. From these corrections weekly mean and standard deviation values were calculated for all stations and the mean value as well as the standard deviation of these values were calculated over the entire evaluation period. These values are listed in Table 12. Compared to values of the combination

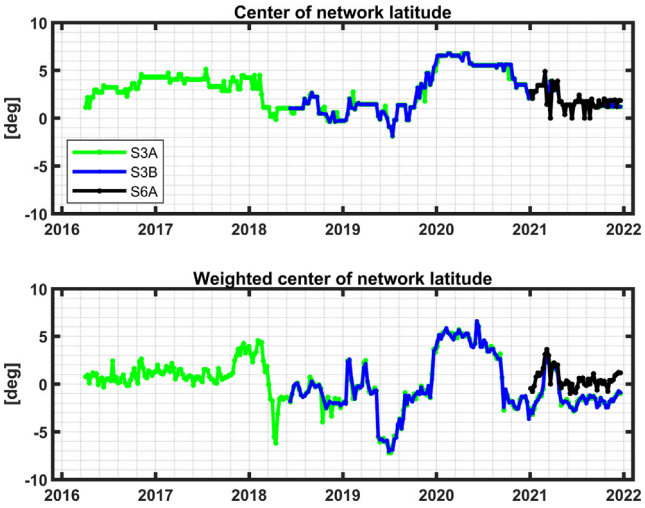

Fig. 9. Center of station network.

solution according to Moreaux et al. (2016) and Moreaux et al. (2023), which show mean weighted RMS values near 1 cm for the three components, the values of the single-satellite solutions and combination are slightly higher. Only in the north and up component values between 1 and 2 cm are reached. The values for the East component are about twice as large with a mean standard deviation of around 2 cm, whereby S6A performs worse. A detailed analysis of the corrections of the station coordinates shows for S6A especially higher deviations near the polar regions. One reason for this could be the lower inclination.

A view of the global distribution of the mean estimated station height corrections is shown for the combined solution in Fig. 10. The most prominent corrections can be seen for Grasse, Syowa and Wettzell with a mean station height correction of about 3 cm. These stations also showed elevated values in the RMS analyses. The height correction values of the remaining stations in the network are significantly lower and do not show any regional or uniform structures.

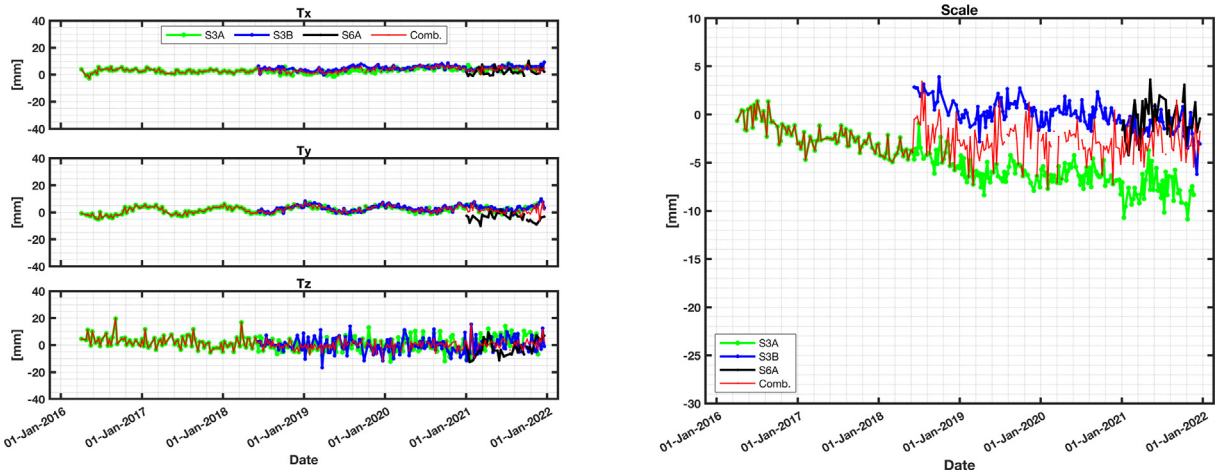

Fig. 8. Translation and scale for the three missions and the combined solution in comparison to a priori.

Table 12
Statistics of estimated station coordinates compared to a priori per arc over the whole timespan. Values are given in mm.

Satellite	East		North		Up	
	Mean	Std.	Mean	Std.	Mean	Std.
Sentinel-3A	10.0 ± 2.4	24.4 ± 5.4	1.9 ± 3.6	13.1 ± 2.0	−4.2 ± 2.6	13.7 ± 6.0
Sentinel-3B	9.0 ± 2.1	22.8 ± 6.2	1.9 ± 3.7	13.2 ± 3.9	0.3 ± 1.8	14.2 ± 4.9
Sentinel-6A	−6.9 ± 3.3	57.7 ± 7.6	0.1 ± 3.7	16.1 ± 3.3	−1.4 ± 2.7	23.6 ± 6.9
Combined Solution	9.0 ± 3.3	22.6 ± 8.8	1.6 ± 2.8	12.0 ± 1.9	−2.0 ± 2.0	13.2 ± 6.1

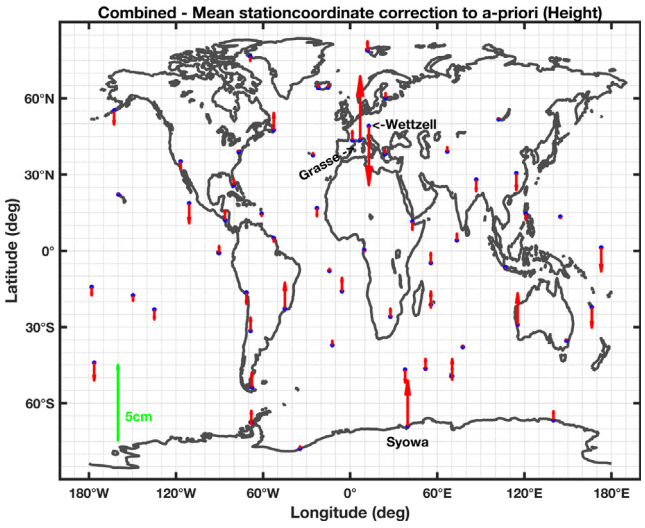

Fig. 10. Mean station height correction of the combined solution with NNR applied.

5. Summary, conclusion and outlook

In this study, we generated orbits for the Sentinel-3A,-3B, and −6A satellites using the techniques DORIS along with SLR, DORIS-only, and GPS-only. The generated orbits were compared with an external reference orbit solution and the accuracy of the orbits was discussed. In the global comparison, no strong systematic deviations were found. Subsequently, the estimation of the DORIS antenna reference point was performed for all three satellites. The Sentinel-3 resulting values show deviations from the used manufacturer values in the mm to cm range, mainly in the radial direction, where a drift of 3 mm per year can be seen. For Sentinel-6A, these correction values are small, indicating good calibration during manufacturing. A multi-technique estimation of the reference points showed radial corrections of the GPS antenna for all three satellites. These corrections would bring the GPS PCO values of the satellites to a common value of 72 mm, which seems reasonable since they are equipped with the same antenna. In normal direction a deviation between the respective reference points of the S3A and S3B satellite of 8–9 mm could be observed, which could indicate a CoM deviation as observed by Montenbruck et al. (2017). Furthermore, for both satellites the DORIS reference point seems to have an additional offset in normal direction of 8–9 mm. The weekly local reference frame solutions generated from this show accuracy values in the mm range for pole coordinates and LOD. By combining the single-satellite solutions at normal equation level, improvements of up to 25% could be achieved here. Compared to combined solutions by the IDS, these values are on a good level. The comparisons of the reference frame in terms of Helmert parameters, which were determined from the changes to a priori, show no significant translations or rotations. Only the scale shows primarily for Sentinel-3A a decreasing trend over time. For Sentinel-3B and −6A, this effect is not quite as noticeable, which is also due to the shorter mission duration. So far we have no explanation for this scale drift. The investigations will continue. In future we strive to expand the suite of orbits for DORIS-equipped missions to most of the altimetry satellites reaching back to the early 1990's and further validate the implemented multi-mission combination environment for single or multi-technique combinations on normal equation level. To in future also be able to more accurately handle time bias effects for DORIS observations, we are also working on a clock correction environment comparable to Štěpánek et al. (2021) fully consistent with EPOS-OC.

Declaration of Competing Interest

The authors declare that they have no known competing financial interests or personal relationships that could have appeared to influence the work reported in this paper.

Acknowledgments

We want to thank the IDS, ILRS, CDDIS and EDC for providing DORIS and SLR observations, the IDS for providing auxiliary documents and satellite specific data. Finally we also want to thank GMV and CPOD (GMV, 2022a) for providing GNSS observation data, satellite meta data, technical notes and especially for providing the combined orbit solutions for this study.

References

Altamimi, Z., 2002. Discussion on How to Express a Regional GPS Solution in the ITRF. In: Report on the Symposium of the IAG Subcommission for Europe (EUREF) in Ponta Delgada, June 5-8, 2002, vol. 12. International Association of Geodesy, pp. 162–167. URL http://www.euref.eu/symposia/book2002/162-167.pdf.

Altamimi, Z., Rebischung, P., Métivier, L., et al., 2016. ITRF2014: A new release of the International Terrestrial Reference Frame modeling

nonlinear station motions. J. Geophys. Res.: Solid Earth 121 (8), 6109–6131. https://doi.org/10.1002/2016jb013098.

Appleby, G., Rodríguez, J., Altamimi, Z., 2016. Assessment of the accuracy of global geodetic satellite laser ranging observations and estimated impact on ITRF scale: estimation of systematic errors in LAGEOS observations 1993–2014. J. Geodesy 90 (12), 1371–1388. https://doi.org/10.1007/s00190-016-0929-2.

Arnold, D., Montenbruck, O., Hackel, S., et al., 2018. Satellite laser ranging to low Earth orbiters: orbit and network validation. J. Geodesy 93 (11), 2315–2334. https://doi.org/10.1007/s00190-018-1140-4.

Biancale, R., Bode, A., 2006. Mean Annual and Seasonal Atmospheric Tide Models Based on 3-hourly and 6-hourly ECMWF Surface Pressure Data. Technical Report STR06/01 Deutsches GeoForschungsZentrum GFZ. https://doi.org/10.2312/GFZ.B103-06011.

Bizouard, C., Lambert, S., Gattano, C., et al., 2018. The IERS EOP 14C04 solution for Earth orientation parameters consistent with ITRF 2014. J. Geodesy 93 (5), 621–633. https://doi.org/10.1007/s00190-018-1186-3.

Boehm, J., Werl, B., Schuh, H., 2006. Troposphere mapping functions for GPS and very long baseline interferometry from European Centre for Medium-Range Weather Forecasts operational analysis data. J. Geophys. Res.: Solid Earth 111 (B02406). https://doi.org/10.1029/2005jb003629.

Capdeville, H., Lemoine, J.-M., 2019. Precise Orbit Determination of DORIS satellites by CNES/CLS IDS Analysis Center in the frame of the next ITRF. Presented at EGU General Assembly 2019, Vienna, Austria.

Cerri, L., Couhert, A., Ferrage, P., 2021. DORIS satellites models implemented in POE processing Ed.: 1/Rev.: 17. Technical Report CNES. URL ftp://ftp.ids-doris.org/pub/ids/satellites/DORISSatelliteModels.pdf.

CNES, 2008. DORIS Data Exchange Format Version 2.2. CNES. https://ids-doris.org/documents/BC/data/doris22.fmt.

CNES, 2022a. Mass and gravity center history for Sentinel-3A/B,6A. URL https://ids-doris.org/analysis-coordination/documents-related-to-data-analysis.html.

CNES, 2022b. RINEX DORIS 3.0 (Issue 1.7). Technical Report CNES. URL ftp://ftp.ids-doris.org/pub/ids/data/RINEX_DORIS.pdf.

Desai, S.D., 2002. Observing the pole tide with satellite altimetry. J. Geophys. Res. 107 (C11), 7-1–7-13. https://doi.org/10.1029/2001jc001224.

Dobslaw, H., Bergmann-Wolf, I., Dill, R., et al., 2017. A new high-resolution model of non-tidal atmosphere and ocean mass variability for de-aliasing of satellite gravity observations: AOD1B RL06. Geophys. J. Int. 211 (1), 263–269. https://doi.org/10.1093/gji/ggx302.

Donlon, C.J., Cullen, R., Giulicchi, L., et al., 2021. The Copernicus Sentinel-6 mission: Enhanced continuity of satellite sea level measurements from space. Remote Sens. Environ. 258, 112395. https://doi.org/10.1016/j.rse.2021.112395.

ESA, 2021. Sentinel-6 POD Context Issue 1 Rev 5. Technical Report ESA. URL ftp://ftp.ids-doris.org/pub/ids/satellites/Sentinel6A_PODcontext.pdf.

Exertier, P., Belli, A., Lemoine, J.-M., 2017. Time biases in laser ranging observations: A concerning issue of Space Geodesy. Adv. Space Res. 60 (5), 948–968. https://doi.org/10.1016/j.asr.2017.05.016.

Ferrari, A.J., 1977. Lunar gravity: A harmonic analysis. J. Geophys. Res. 82 (20), 3065–3084. https://doi.org/10.1029/jb082i020p03065.

Folkner, W.M., Williams, J.G., Boggs, D.H., et al., 2014. The Planetary and Lunar Ephemerides DE430 and DE431. The Interplanetary Network Progress Report, 42–196.

GMV, 2022a. Copernicus POD Regular Service Review Jan. – Dec. 2021. Technical Report GMV. https://sentinels.copernicus.eu/web/sentinel/technical-guides/sentinel-3-altimetry/pod/documentation.

GMV, 2022b. SENTINEL-3 PROPERTIES FOR GNSS POD. Technical Report GMV. https://sentinels.copernicus.eu/documents/247904/322310/GMV-CPOD-TN-0027_v2.0_Sentinel-3+properties+for+GPS+POD.pdf.

Hedin, A.E., 1991. Extension of the MSIS Thermosphere Model into the middle and lower atmosphere. J. Geophys. Res.: Space Phys. 96 (A2), 1159–1172. https://doi.org/10.1029/90ja02125.

ILRS, 2020. SLRF 2014 version: 2030 from 200428. https://cddis.nasa.gov/archive/slr/products/resource/SLRF2014_POS+VEL_2030.0_200428.snx.

Jäggi, A., Dach, R., Montenbruck, O., et al., 2009. Phase center modeling for LEO GPS receiver antennas and its impact on precise orbit determination. J. Geodesy 83 (12), 1145–1162. https://doi.org/10.1007/s00190-009-0333-2.

Johnston, G., Riddell, A., Hausler, G., 2017. The International GNSS Service. In: Springer Handbook of Global Navigation Satellite Systems. Springer International Publishing, Basel, Switzerland, pp. 967–982. https://doi.org/10.1007/978-3-319-42928-1_33.

König, R., Reinhold, A., Dobslaw, H., et al., 2021. On the effect of non-tidal atmospheric and oceanic loading on the orbits of the altimetry satellites ENVISAT, Jason-1 and Jason-2. Adv. Space Res. 68 (2), 1048–1058. https://doi.org/10.1016/j.asr.2020.05.047.

Kvas, A., Brockmann, J.M., Krauss, S., et al., 2021. GOCO06s – a satellite-only global gravity field model. Earth Syst. Sci. Data 13 (1), 99–118. https://doi.org/10.5194/essd-13-99-2021.

Lemoine, J.-M., 2014. Routines to read DORIS/RINEX files (courtesy by Jean-michel Lemoine, CNES). URL ftp://ftp.ids-doris.org/pub/ids/-data/DORIS_RINEX_subroutines_from_GINS.tar.

Lemoine, J.-M., Capdeville, H., Soudarin, L., 2016. Precise orbit determination and station position estimation using DORIS RINEX data. Adv. Space Res. 58 (12), 2677–2690. https://doi.org/10.1016/j.asr.2016.06.024.

Luzum, B., Petit, G., 2012. The IERS Conventions (2010): reference systems and new models. Proc. Int. Astron. Union 10 (H16), 227–228. https://doi.org/10.1017/s1743921314005535.

Lyard, F.H., Allain, D.J., Cancet, M., et al., 2021. FES2014 global ocean tide atlas: design and performance. Ocean Sci. 17 (3), 615–649. https://doi.org/10.5194/os-17-615-2021.

Mendes, V.B., Pavlis, E.C., 2004. High-accuracy zenith delay prediction at optical wavelengths. Geophys. Res. Lett. 31 (L14602). https://doi.org/10.1029/2004gl020308.

Michalak, G., König, R., Dahle, C., 2017. GPS-based LEO orbit determination with carrier phase cycle slip fixing over long data gaps. Presented at IGS Workshop 2017, Paris, France. https://gfzpublic.gfz-potsdam.de/pubman/item/item_5004507.

Montenbruck, O., Hackel, S., Jäggi, A., 2017. Precise orbit determination of the Sentinel-3A altimetry satellite using ambiguity-fixed GPS carrier phase observations. J. Geodesy 92, 711–726. https://doi.org/10.1007/s00190-017-1090-2.

Montenbruck, O., Hackel, S., Wermuth, M., et al., 2021. Sentinel-6A precise orbit determination using a combined GPS/Galileo receiver. J. Geodesy 95. https://doi.org/10.1007/s00190-021-01563-z.

Moreaux, G., Lemoine, F.G., Capdeville, H., et al., 2016. The International DORIS Service contribution to the 2014 realization of the International Terrestrial Reference Frame. Adv. Space Res. 58 (12), 2479–2504. https://doi.org/10.1016/j.asr.2015.12.021.

Moreaux, G., Lemoine, F.G., Capdeville, H., et al., 2023. The international DORIS service contribution to ITRF2020. Adv. Space Res. 72 (1), 65–91. https://doi.org/10.1016/j.asr.2022.07.012.

Moreaux, G., Willis, P., Lemoine, F.G., et al., 2019. DPOD2014: A new DORIS extension of ITRF2014 for precise orbit determination. Adv. Space Res. 63 (1), 118–138. https://doi.org/10.1016/j.asr.2018.08.043.

Noll, C.E., 2010. The crustal dynamics data information system: A resource to support scientific analysis using space geodesy. Adv. Space Res. 45 (12), 1421–1440. https://doi.org/10.1016/j.asr.2010.01.018.

Noll, C.E., Ricklefs, R., Horvath, J., et al., 2018. Information resources supporting scientific research for the international laser ranging service. J. Geodesy 93, 2211–2225. https://doi.org/10.1007/s00190-018-1207-2.

Pearlman, M.R., Noll, C.E., Pavlis, E.C., et al., 2019. The ILRS: approaching 20 years and planning for the future. J. Geodesy 93, 2161–2180. https://doi.org/10.1007/s00190-019-01241-1.

Peter, H., Sánchez, J.F., Gallardo, L.J. et al., 2018. Copernicus POD Service - Sentinel-3 orbit determination based on DORIS observation. Presented at IDS Workshop 2018, Ponta Delgada, São Miguel Island, Azores Archipelago, Portugal. URL https://ids-doris.org/images/documents/report/ids_workshop_2018/IDS18_s3_Peter_CPODserviceSentinel3.pdf.

Petit, G., & Luzum, B. (2010). IERS Technical Note No. 36. Frankfurt am Main, Germany: Verlag des Bundesamts für Kartographie und Geodäsie. URL https://www.iers.org/IERS/EN/Publications/TechnicalNotes/tn36.html.

Ries, J., 2017. Conventional Model Update for Rotational Deformation. In: Presented at AGU Fall Meeting 2017, New Orleans, Louisiana, USA. https://doi.org/10.26153/TSW/2659.

Rudenko, S., Neumayer, K.-H., Dettmering, D., et al., 2017. Improvements in Precise Orbits of Altimetry Satellites and Their Impact on Mean Sea Level Monitoring. IEEE Trans. Geosci. Remote Sens. 55 (6), 3382–3395. https://doi.org/10.1109/tgrs.2017.2670061.

Schrama, E., 2018. Precision orbit determination performance for CryoSat-2. Adv. Space Res. 61 (1), 235–247. https://doi.org/10.1016/j.asr.2017.11.001.

Schreiner, P., König, R., Michalak, G., 2021. Precise orbit determination of low Earth orbiters using carrier phase cycle slip fixing over long data gaps - an alternative to GNSS phase bias products based ambiguity resolution. In: Presented at 43rd COSPAR Scientific Assembly, Sydney, Australia.

Schwatke, C., 2012. EUROLAS Data Center (EDC) - A new website for tracking the SLR data flow. Presented at EGU General Assembly 2012, Vienna, Austria.

Štěpánek, P., Hugentobler, U., Filler, V., et al., 2021. Correction to: Inclusion of GPS clock estimates for satellites Sentinel-3A/3B in DORIS geodetic solutions. J. Geodesy 95. https://doi.org/10.1007/s00190-021-01573-x.

Wahr, J.M., 1981. The forced nutations of an elliptical, rotating, elastic and oceanless earth. Geophys. J. Roy. Astron. Soc. 64 (3), 705–727. https://doi.org/10.1111/j.1365-246x.1981.tb02691.x.

Willis, P., Lemoine, F.G., Moreaux, G., et al., 2015. The International DORIS Service (IDS): Recent Developments in Preparation for ITRF2013. In: Rizos, C., Willis, P. (Eds.), IAG 150 Years. International Association of Geodesy Symposia, vol. 143. Springer, Cham, Switzerland, pp. 631–640. https://doi.org/10.1007/1345_2015_164.

Zelensky, N.P., Berthias, J.-P., Lemoine, F.G., 2006. DORIS time bias estimated using Jason-1, TOPEX/Poseidon and ENVISAT orbits. J. Geodesy 80, 497–506. https://doi.org/10.1007/s00190-006-0075-3.

Zhu, S., Reigber, C., König, R., 2004. Integrated adjustment of CHAMP, GRACE, and GPS data. J. Geodesy 78, 103–108. https://doi.org/10.1007/s00190-004-0379-0.